Broadband HF backscattering from a smooth sand surface

Charles F. Greenlaw and D. V. Holliday
BAE SYSTEMS Applied Technologies, Inc.
4669 Murphy Canyon Road
San Diego CA 92123

Measurements of backscattering from smoothed sand surfaces at frequencies from 200 kHz to 4 MHz and grazing angles from 20 to 80 degrees were made in a laboratory tank. The sand was a well-sorted fine sand with all organics and shell fragments removed. The surface was smoothed prior to making measurements at multiple locations using three different broadband transducers (0.5, 1.0, and 2.25 MHz) driven by an impulse. Waveforms from 32-ping coherent averages were recorded, the spectra averaged and normalized by the transducer beamwidths (as an analog for ensonified area), and joined to produce a relative backscattering spectrum for the sand surface at each grazing angle. The results suggest that scattering [from smooth surfaces, n.b.] is mediated by sand-grain-scale roughness at high frequencies and is reasonably consistent with Lambert's Rule up to near-normal incidence. At lower frequencies, the scattering strength jumps abruptly higher at grazing angles above about 50 degrees, which is consistent with some models for volume scattering. [Work supported by ONR.]

Previously-reported measurements of high-frequency backscattering from sandy bottoms have shown a frequency-dependence that suggested a connection with grain-size roughness (Fig. 1; Greenlaw et al., 2004,). The roll-off in Lambert's Parameter observed in the SAX-99 field trials was originally ascribed to a transition from ripple-structure-controlled to grain-size-controlled scattering as frequency increased. Comparisons of the field data to laboratory data taken by Williams, et al. (1988) on sand and glass bead surfaces suggested a link with grain size but the sand data were inconsistent with existing models for scattering from individual sand grains (Holliday, 1987).

An opportunity arose in 2003 to obtain laboratory data on sand sediments over similar frequency ranges to the field data but under more controlled circumstances. A plywood box was constructed to contain beach sand collected from Ocean Beach at San Diego, CA. This box, 86 X 147 x 10 cm deep was suspended in a small test tank filled with chlorinated, filtered fresh water. The beach sand was washed in small batches and all visible organic detritus removed. There were relatively few shell fragments in this sample; those observed were removed by hand. Each batch of saturated sand was vacuum degassed underwater and then carefully decanted underwater into the box. Every effort was made to preclude the presence of bubbles in the sand samples. The test tank temperature varied only slightly over the duration of the experiment (20-23C)

A carriage (Fig. 2) was fabricated to hold broadband transducers (Panametrics immersion models) at measured grazing angles above the tank. The carriage rode on large pulleys, acting as wheels, along a pair of metal rods acting as tracks. The tracks permitted the carriage to be easily moved across the sand bed to obtain scattering data from different sand patches at the same grazing angle and height. The entire track/carriage assembly could be moved laterally to permit measurements on a new swath of sand. The centers of the transducers were approximately 13.3 cm above the sand bed. Measurements

were taken at 10-12 different locations in the tank spaced 75mm along the track and 300mm horizontally.

The sand was left to settle for several weeks prior to the initial measurements. During this time, simple physical measurements on the sand were made.

A sample of the sand was sent to NRL Stennis where it was screened and sized by Kevin Briggs. The sand was described as well-sorted fine sand with a mean φ of 2.07 or a mean diameter of 0.24 mm.

Density was estimated by weighing a measured volume of fresh-water-saturated sand. The sand was packed by tapping the beaker on a bench top until the settled volume remained constant. Excess water was removed before weighing. The estimated density was 1999 kg/m^3, similar to that found in sandy bottoms off San Diego (2010 kg/m^3; Hamilton, et al., 1970) and slightly lower than the mean density for the West Destin sanded where the field measurements were taken (2074 kg/m^3; Richardson et al., 2001).

Sound velocities were measured in a T-tube velocimeter originally developed for measuring zooplankton sound speeds (Greenlaw, 1977; Foote, 1990). The apparatus consists of a frame holding a 2.25 MHz broadband transducer at one end of a horizontal plexiglas tube. A stainless steel rod with a polished face serving as a reflector closes the other end of the tube, forming a cylindrical chamber with fixed length. A second piece of plexiglas tube is attached vertically at right angles to the horizontal tube to allow filling the chamber with water or sand. The same pulser used in the scattering measurements was used to drive the velocimeter transducer. Measurement of the time of flight for the broadband pulse with fresh water in the chamber provided a baseline estimate of the effective path length of the chamber (66.64 mm one-way). Sound speed was calculated from the Wilson (1959) equation for fresh water at the measured temperature (1487 m/sec). Sand was then added and stirred until the chamber was essentially packed with sand and the time of

flight measured again. Using the effective pathlength measured in water, sound speed was estimated at 1674 m/sec.

The attenuation in the sand was extremely high at the center frequency of the transducer used. Based simply on peak to peak amplitudes of the reflected signals, excess attenuation over the 133.2 mm total path was about 55 dB. Examination of the waveforms (Fig. 3) shows that the high-frequency components of the water-borne signal are essentially missing from the signal measured through the sand, consistent with the presumption that absorption and attenuation in saturated sand increases with frequency.

From these measurements of the physical properties, the critical angle for the laboratory sand bed was estimated to be 27°. The Rayleigh reflection coefficient was calculated to be 0.386 for a bottom loss at normal incidence of 8.3 dB.

ACOUSTIC RESULTS

Previous high-frequency measurements on water-saturated sand (Nolle et al., 1963) emphasized the importance of obtaining a perfectly plane surface to obtain valid scattering data. In this experiment, it was hoped that averages of multiple independent trials on an approximately plane surface would produce meaningful results. Visual checks for ripples included illuminating the surface with the beam from an inexpensive laser-level device equipped with a cylindrical lens to produce a line of light. (A similar scheme was employed on a submersible by Chotiros et al., ARL/UT, during SAX-99, from which this idea was obtained.) Refraction caused the line of light that emerged underwater to form an arc that could be directed at the bottom. Holding the laser source at an angle of approximately 45°, ripples showed up as wiggles in this line. Since the line was well under 1 mm in width, it was possible to see ripples of about this size and larger. The sand surface was scraped and checked until the entire usable surface appeared ripple-free.

The transducers were driven by a high-voltage pulser-receiver system (Panametrics 5077PR), producing short, broadband signals in the water. The transducers were used as both source and receiver. Data were recorded on a digital oscilloscope. A built-in function was used to obtain coherent averages of 32 pings for each waveform recorded. Waveforms were sampled at 25 MHz; amplitude resolution was 8 bits (nominally 10 bits in averaging mode). Echoes were obtained from eight to twelve locations in the sand box using three different transducers with nominal center frequencies of 0.5, 1.0, and 2.25 MHz. Usable spectral data were obtained from about 200 kHz to 4 MHz.

The rather narrow beam pattern of the transducers intersecting with the planar surface produced a time-limited echo from the sand bottom such as that shown in Fig. 4 (upper). It was observed that the echo structure within the envelope formed by the intersection of the beam with the bottom was deterministic and fixed, in the sense that moving the carriage slowly over the sand surface caused echo highlights to move through the echo region in synchrony with the carriage movement. Had the signal been composed of random-phase replicas of the transmit waveform, each movement of the carriage in excess of half a pulselength would have produced a new realization of a random composite waveform. The length of the ensonified region was on the order of 200 mm while the total pulse lengths were on the order of 3 mm or less. Thus, each highlight in the echo structure apparently arose from some sort of facet or feature on the sand bed; possibly from micro-ripples introduced by the leveling process. A section of the echo corresponding to 50mm pathlength centered on the intersection of the beam center with the sand surface was selected for processing (Fig. 4 upper, horizontal bar).

System response was measured by suspending the transducers inverted below the air-water interface and recording the echoes from the still surface (Patterson 1967, Bobber 1970). Receiving gain was reduced 40 dB for these data. Other than gain, the bottom scattering signals were recorded using the

same settings as the surface scattering data and ranges were similar. Hence, dividing the echo spectra by the surface reciprocity spectra and correcting for the gain changes served to normalize the echo spectra into backscattering spectra. An example of the raw echo spectrum and the normalized backscattering spectrum taken at a grazing angle of 20° is shown in Fig 4 (middle and lower). The intensity spectra produced by each individual transducer from each area were averaged and the resultant mean spectrum smoothed with a 5-point boxcar filter. These three smoothed spectra are shown in Fig. 5.

Since the signals used in this experiment were extremely short and broadband, the sonar equation approach was deemed inappropriate for adjusting these data. Instead, a simple adjustment for the finite apertures of each transducer was made by scaling the data. The -6 dB beamwidth, θ, of a piston transducer can be approximated by

$$\sin(\theta/2) \cong \frac{0.514c}{fD}$$

where c is the speed of sound, f the frequency, and D the diameter of the piston. The effective ensonified area is proportional to this angle, viz.

$$A \approx \frac{c\tau}{2} R \sin(\theta_{-3dB})$$

$$A \propto \sin(2\tan^{-1}(\frac{0.514c}{fD})$$

Dividing the spectra by this correction factor introduces 'tilt' into each spectrum that improves the fit at the ends of the spectra as shown in Fig. 6. In this figure, a composite spectrum was created by averaging the individual spectral intensities where two spectra overlapped. This correction is sufficient to obtain a realistic spectral shape for the surface scattering but, since the actual ensonified area is not calculated, does not produce an estimate of actual surface scattering

strength. These results were considered adequate, however, for addressing the question of grain-size dependence.

While different from the results from the field data, the shape of the lab data spectrum does resemble the scattering curve from sand grains obtained empirically by Sheng (1991; also cited in Crawford and Hay 1993) from data on sand particles in a turbulent jet (Hay 1991). Using a sand grain size of 0.25 mm average diameter, the form factor for an individual sand grain was computed with this model. This model is overlaid on the measured sanded spectrum in Fig 6. An arbitrary scale factor was added to make the curves coincide. It is evident from the comparison that the shapes of these curves are quite similar, suggesting that the high-frequency portion of the sanded scattering is largely dominated by the sizes of the sand grains themselves, although the estimate of the mean grain size from visual fitting is relatively crude. While there is no reason to presume that the scattering from a half-space of well-sorted saturated sand should behave like the scattering from an individual sand grain of the mean size, the correlation is quite striking.

Note, however, the portion of the sanded spectrum below about 400 kHz. There is a definite departure from the individual sand grain model at this point and the frequency dependence -- which should approach f^4 for the Rayleigh region of an individual scatterer -- is on the order of f^1. This is more consistent with low-frequency results from sand bottoms where the frequency dependence ranges from f^1 to $f^{1.6}$.

The sand bed had been constructed by gently pouring the saturated sand batches into the box. No particular attempt was mad to pack the sand, although the filled box was left for several weeks before measurements began. Thus, it seemed likely that the porosity of the surficial sand was probably quite high. To investigate this possibility, a vibrator was constructed from an AC motor fitted with an eccentric mass load on the output shaft (Fig. 7). This vibrator was clamped to the sand box and operated for approximately 12 hours over two days

to compact the sand. The sand surface became noticeably firmer to the touch after only an hour or so of vibration. The surface was scraped flat again about half-way through the compaction process.

A complete set of duplicate data was taken from this compacted sand surface. It was noticed that the vertical distance to the sand bed from the transducers had increased slightly upon compaction of the sand -- by about 1.0-1.5 cm. Data processing proceeded identically to the unpacked sand case, resulting in the curve shown in Fig. 8. The data from the unpacked sand are shown for comparison. The differences between the curves is minimal above about 500 kHz; these differences are probably explained by the slightly different slant ranges to the bottom due to the different heights. Note, however, that the low frequency tail of the spectrum now continues to decrease with decreasing frequency. This difference is ascribed to the lower porosity of the compacted sand bed. It is also possible that the surface was somewhat smoother in the case of the compacted sand bed.

The spectrum for compacted sand is compared to the Sheng model in Fig. 9. Again, there is rather good agreement between the measurements and this model above 500 kHz. Below this frequency, the measured backscattering exceeds the fitted model curve. This might be taken as evidence that, at least below the critical angle and for low frequencies, another scattering mechanism is equally, or more, important than grain size. It is relevant to keep in mind that these results are for artificially smooth sand surfaces.

To investigate the changes in scattering behavior with frequency, data at fixed frequencies were abstracted from the composite mean spectra at the various grazing angles and plotted along with curves embodying the Lambert's Rule function (Fig. 10). The spectral points at high frequencies appear to follow Lambert's Rule with acceptable precision. The low-frequency data tend to depart from this behavior at steeper grazing angles, above about 50° (well above the critical angle). This would appear to indicate that a different mechanism is

controlling the scattering in this region. A similar behavior with grazing angle was found by Ivakin and Lysanov (1981) for shallow-water scattering at 100 kHz.

This transition in scattering mechanisms can be illustrated in another way. The composite mean spectra were adjusted in level by applying Lambert's Rule to the each spectrum and the resulting spectra plotted versus frequency (Fig. 11). Where Lambert's Rule applies, the spectra should overlay. To reasonable precision, this occurs for all data above about 50° grazing angle and to all data above about 2 MHz. Below about 500 kHz, the shallow grazing angle data depart sharply from the other curves -- based upon Fig. 10, this is taken as evidence that the scattering mechanism is no longer dominated by grain-size roughness.

In addition, the low-grazing-angle data also diverge visibly from the other spectra between about 500 kHz and 2 MHz. This may or may not be significant in light of the 2dB or so fluctuations of the various spectra about the presumed mean value.

CONCLUSIONS

Field measurements of shallow-grazing-angle backscattering from a sandy bottom at frequencies bracketing 1 MHz showed a resonance-like peak structure at a frequency that appeared to be weakly-related to the mean grain size. Coherent processing of laboratory measurements on relatively flat sand beds at sub-critical grazing angles produced a backscattering spectrum that was a close fit to a model for individual sand grains (Sheng, 1991; Crawford and Hay 1993). The mean size that gave a visual fit to the measured spectrum was 0.25 mm. Thus, it seems clear that the sand grain size is an important limiting factor in the backscattering process for sand surfaces. Since surface roughness is limited at small scales by the sizes of the sand grains, this result is hardly surprising.

Porosity effects for this smooth surface were limited to frequencies below 500 kHz. The un-compacted sand had higher backscattering strengths in this region than did the compacted sand.

At low grazing angles , the scattering behavior deviates from the extrapolated behavior at higher grazing angles, implying a shift in the dominant scattering mechanism.

ACKNOWLEDGEMENTS

This work was conducted with the sponsorship of the Office of Naval Research (under Contract Nos. N00014-980C-0442 and N00014-00-D-0122). Much of the laboratory setup and data collection was performed by summer interns, Jeremy Roswell and Eugene Smith, whose efforts are gratefully acknowledged.

REFERENCES

Bobber, R. J. (**1970**). *Underwater Electroacoustic Measurements*. U. S. Gov't Printing Office. 325 pp.

Boehme, H. N., N. P. Chotiros, L. D. Rolleigh, S. P. Pitt, A. L. Garcia, T. G. Goldsberry, and R. A. Lamb (**1985**). "Acoustic backscattering at low grazing angles from the ocean bottom: Part I. Bottom backscatter strength," J. Acoust. Soc. Am 77(3): 962-974.

Boehme, H. N. and N. P. Chotiros (**1988**). "Acoustic backscattering at low grazing angles from the ocean bottom," J. Acoust. Soc. Am 84(3): 1018-1029.

Crawford, A. M. and A. E. Hay (**1993**). "Determining suspended sand size and concentration from multifrequency acoustic backscatter," J. Acoust. Soc. Am. 94(6): 3312-24.

Foote, K. G. (**1990**). "Speed of sound in *Euphausia superba*," J. Acoust. Soc. Am. 87(4): 1405-8.

Greenlaw, C. F. (**1977**). "Backscattering spectra of preserved zooplankton," J. Acoust. Soc. Am. 62(1): 44-52.

Greenlaw, C. F. and D. V. Holliday (**2004**). High-frequency scattering from saturated sand sediments. J. Acoust. Soc. Am. 115(6): 2818-2823.

Hamilton, E. L, H. P. Bucker, D. L. Keir and, J. A. Whitney (**1970**). "Velocities of compressional and shear waves in marine sediments determined in situ from a research submersible," J. Geo. Res. 75(20): 4039-4049.

Hay, A. E. (**1991**). "Sound scattering from a particle-laden, turbulent jet," J. Acoust. Soc. Am. 90(4): 2055-74.

Holliday, D. V. (**1987**). "Acoustic determination of suspended particle size spectra." In Coastal Sediments '87 Volume 1, WW Div./ASCE, New York: 260-272.

Ivakin, A.N. and Yu. P. Lysanov (**1981**). "Underwater sound scattering by volume inhomogeneities of a bottom medium bounded by a rough surface." Sov. Phs. Acoust. 27(3): 212-215.

Jackson, D. R., A. M. Baird, J. J. Crisp, and P. A. G. Thomason (**1986**). "High-frequency bottom backscattering measurements in shallow water," J. Acoust. Soc. Am 80(4): 1188-1199.

Jackson, D. R. and K. B. Briggs (**1992**). "High-frequency bottom backscattering: Roughness versus sediment volume scattering," J. Acoust. Soc. Am. 92(2): 962-977.

Johnson, R. K. (**1977**). "Acoustic estimation of scattering-layer composition," J. Acoust. Soc. Am. 61(6): 1636-9.

Lawson, C. L. and R. J. Hanson (**1974**). *Solving Least Squares Problems*. Prentice-Hall, Inc. Englewood Cliffs, N.J.

MacKenzie, K. V. (**1961**). "Bottom reverberation for 530- and 1030-cps sound in deep water," J. Acoust. Soc. Am. 33(11): 1498-1504.

McKinney, C. M. and W. D. Anderson (**1964**). "Bottom backscattering near grazing incidence in shallow water," J. Acoust. Soc. Am 36(1): 158-163.

Nolle, A. W., W. A. Hoyer, J. F. Mifsud, W. R. Runyan, and M. B. Ward (**1963**). "Acoustical properties of water-filled sands," J. Acoust. Soc. Am 35(9): 1394-1408.

Patterson, R. B. (**1967**). "Using the ocean surface as a reflector for a self-reciprocity calibration of a transducer," J. Acoust. Soc. Am. 42(3): 653-655.

Richardson, M. D., K. B. Briggs, L. D. Bibee, P. A. Jumars, W. B. Sawyer, D. B. Albert, R. H. Bennett, T. K. Berger, M. J. Buckingham, N. P. Chotiros, P. H. Dahl, N. T. Dewitt, P. Fleisher, R. Flood, C. F. Greenlaw, D. V. Holliday, M. H. Hurlbert, M. P. Hutnak, P. D. Jackson, J. S. Jaffe, H. P. Johnson, D. L. Lavoie, A. P. Lyons, C. S. Martens, D. E. McGehee, K. D. Moore, T. H. Orsi, J. N. Piper, R. I. Ray, A. H. Reed, R. F. L. Self, J. L Schmidt, S. G. Schock, F. Simonet, R. D. Stoll, D. Tang, D. E. Thistle, E. I. Thorsos, D. J. Walter, and R. A. Wheatcroft (**2000**). "Overview of SAX99: Environmental considerations," I.E.E.E J. Ocean. Engr. 26(1): 26-53.

Sheng, J. (**1991**). "Remote Determination of Suspended Sediment Size and Concentration by Multi-frequency Acoustic Backscatter," Ph.D. thesis, Dept. of Physics, Memorial University of Nfld.

Stanic, S., K. B. Briggs, P. Fleishcer, R. I. Ray, and W. B. Sawyer (**1988**). "Shallow-water high-frequency bottom scattering off Panama City, Florida," J. Acoust. Soc. Am. 83(6): 2132-2144.

Stanic, S., K. B. Briggs, P. Fleischer, W. B. Sawyer, and R. I. Ray (**1989**). "High-frequency acoustic backscattering from a coarse shell ocean bottom," J. Acoust. Soc. Am 85(1): 125-136

Tang, D., G. Jin, D. R. Jackson, and K. L. Williams (**1994**). "Analyses of high-frequency bottom and subbottom backscattering for two distinct shallow water environments," J. Acoust. Soc. Am. 96(5): 2930-2936.

Thorsos, E. I., K. L. Williams, N. P. Chotiros, J. T. Christoff, K. W. Commander, C. F. Greenlaw, D. V. Holliday, D. R. Jackson, J. L. Lopes, D. E. McGehee, J. E. Piper, M. D. Richardson, and D. Tang (**2000**). "An overview of SAX99: Acoustic measurements," I.E.E.E J. Ocean. Engr. 26(1): 4-25.

Urick, R. J. (**1954**). "The backscattering of sound from a harbor bottom," J. Acoust. Soc. Am. 26(2): 231-5.

Urick, R. J. (**1967**). *Principles of Underwater Sound for Engineers*. McGraw-Hill, New York.

Urick, R. J. (**1970**). "Reverberation-derived scattering strength of the shallow sea bed," J. Acoust. Soc. Am 48(1): 392-397.

Williams, K. L., R. H. Hackman, and D. H. Trivett (**1988**). "High-frequency scattering from liquid/porous sediment interfaces," J. Acoust. Soc. Am 84(2): 760-770.

Wilson, W. D. (**1959**). "Speed of Sound in Distilled Water as a Function of Temperature and Pressure," J. Acoust. Soc. Am. 31(8): 1067-1072.

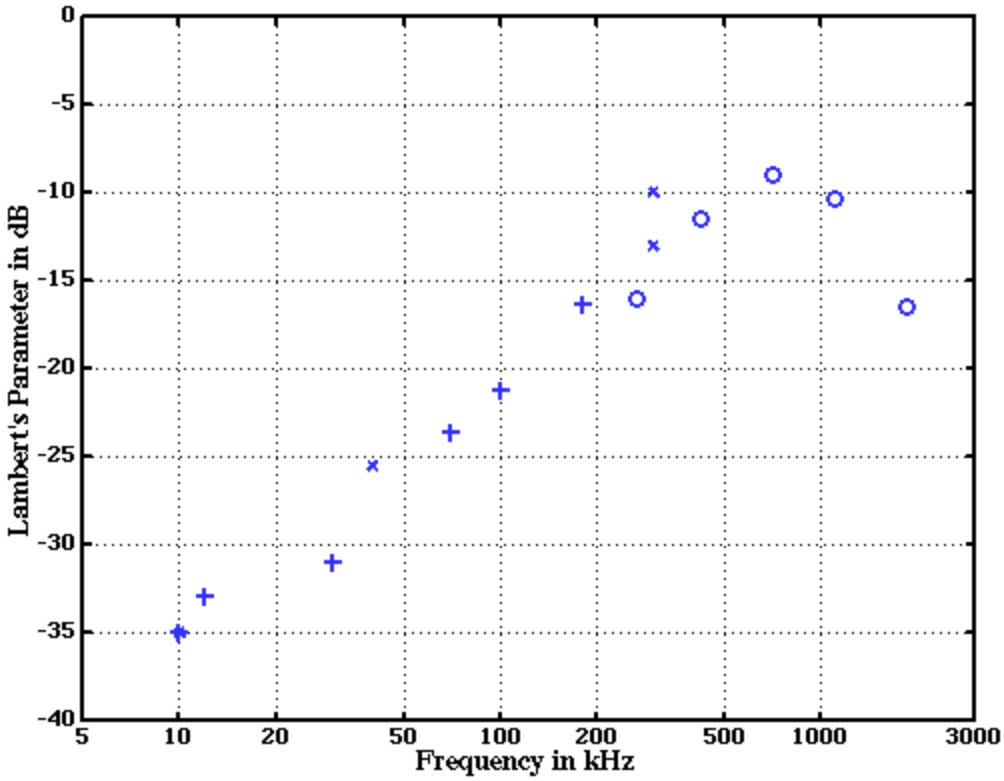

Figure 1. Mean normalized backscattering strength (Lambert's parameter) versus frequency for similar sandy sea beds. Data key: (o) SAX-99 TAPS-8 data; (x) BAMS data from SAX-99 (K. Williams, pers. comm.); (*) Muir, as reported by Boehme and Chotiros (1988); (+) medium sand data from McKinney and Anderson (1964). The TAPS-8 data were reported in Greenlaw et al., 2004.

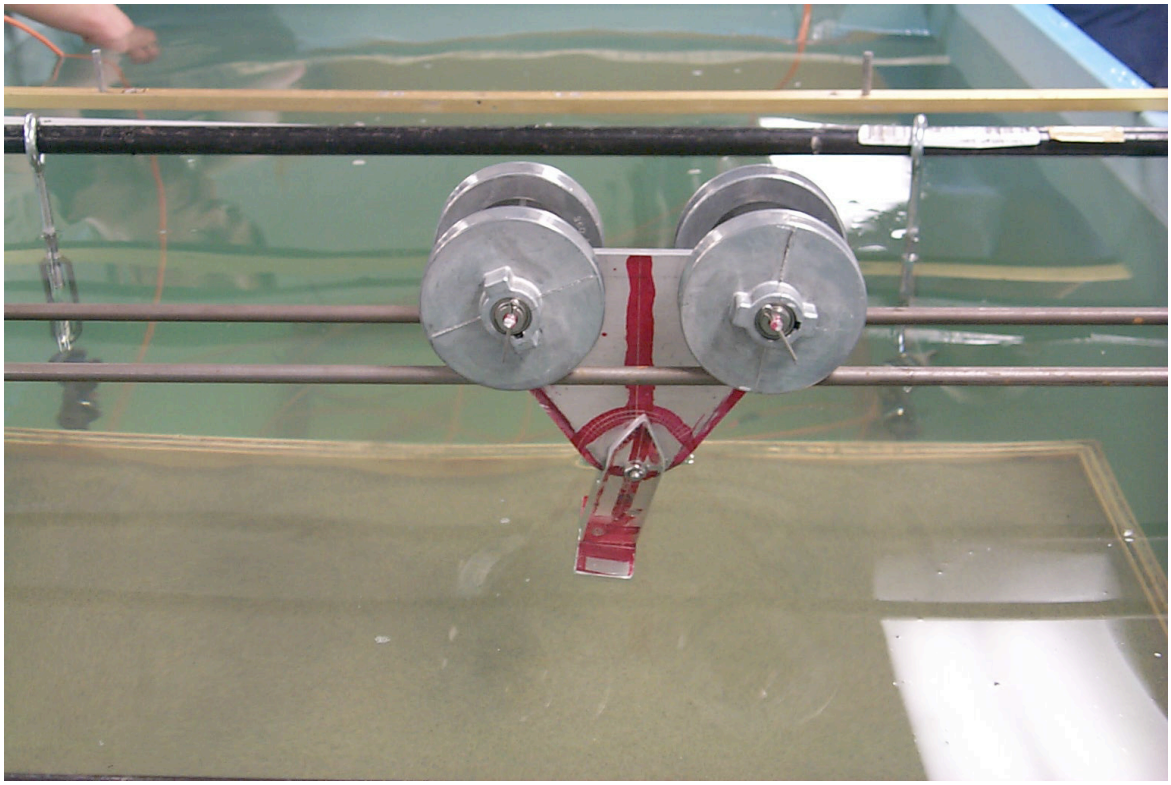

Figure 2. Photograph of the carriage assembly on the horizontal tracks above the sanded in the test tank. The T-shaped portion attached to the bottom of the carriage with a through-bolt holds two broadband transducers (not shown) and can be adjusted to any grazing angle desired. The plywood box (under water) holds a bed of vacuum-degassed sand for this study. Turnbuckles allow the box to be leveled beneath the transducer carriage.

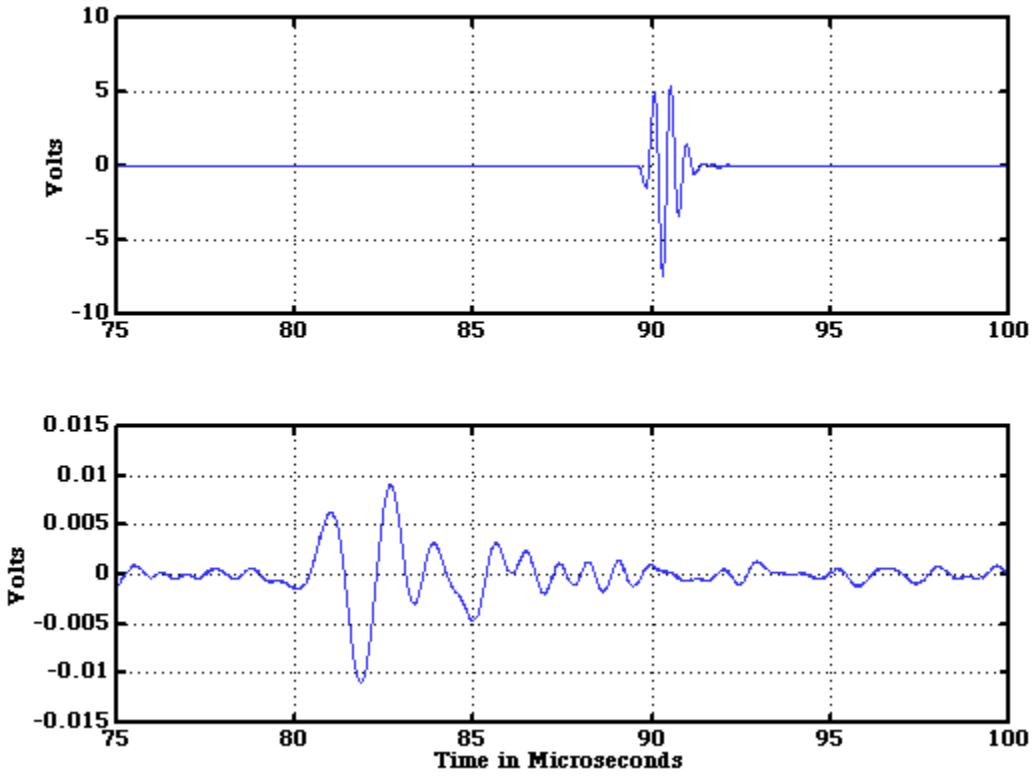

Figure 3. Waveforms from the T-tube velocimeter for fresh water (top panel) and fresh-water-saturated sand (lower panel). The source is a 2.25 MHz broadband transducer impulsively driven. The signal is reflected by the end of a steel rod and received by the same transducer. The two-way path length is 133.3 mm. Sound speed was estimated by the ratio of travel times and the sound speed for fresh water calculated by the Wilson (1959) equation. Note the nearly complete loss of high-frequency energy due to the high attenuation in saturated sand.

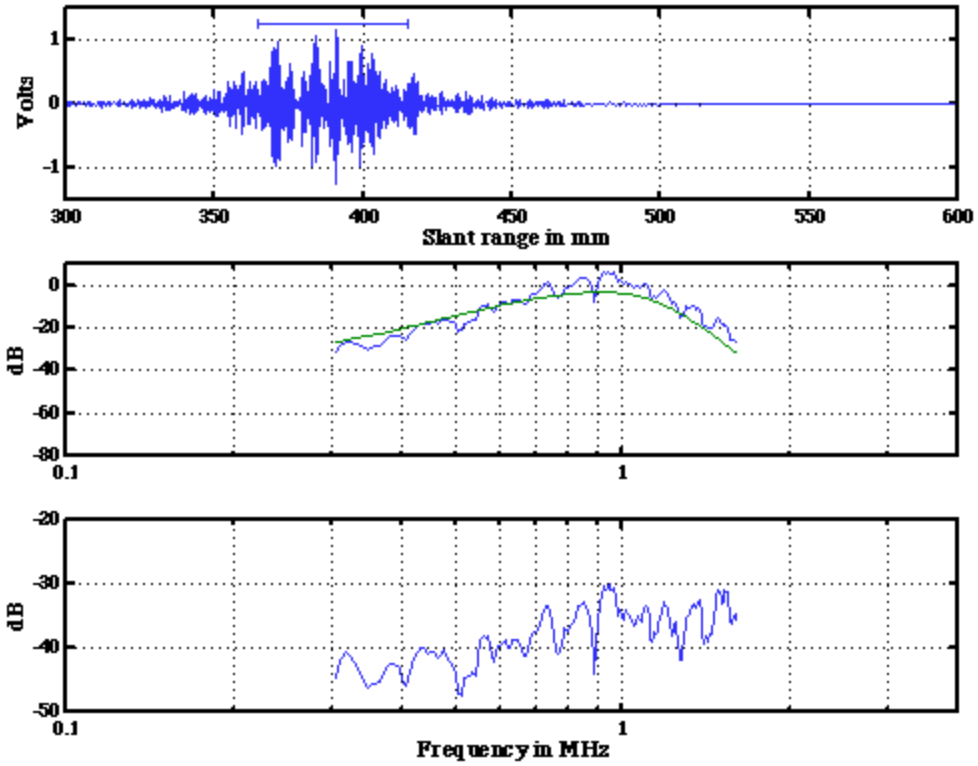

Figure 4. Typical broadband echo from sand surface at 20° grazing angle using the 1.0 MHz source. The echo formed by a 32-ping coherent average of backscattered signals is shown in the upper panel with the section selected for analysis marked by a horizontal line segment. The smoothed spectrum of this signal is shown in the middle panel along with the surface-reciprocity system response spectrum (smooth curve). The ratio of the echo spectrum to the system response spectrum, corrected for system gains, is shown in the lower panel.

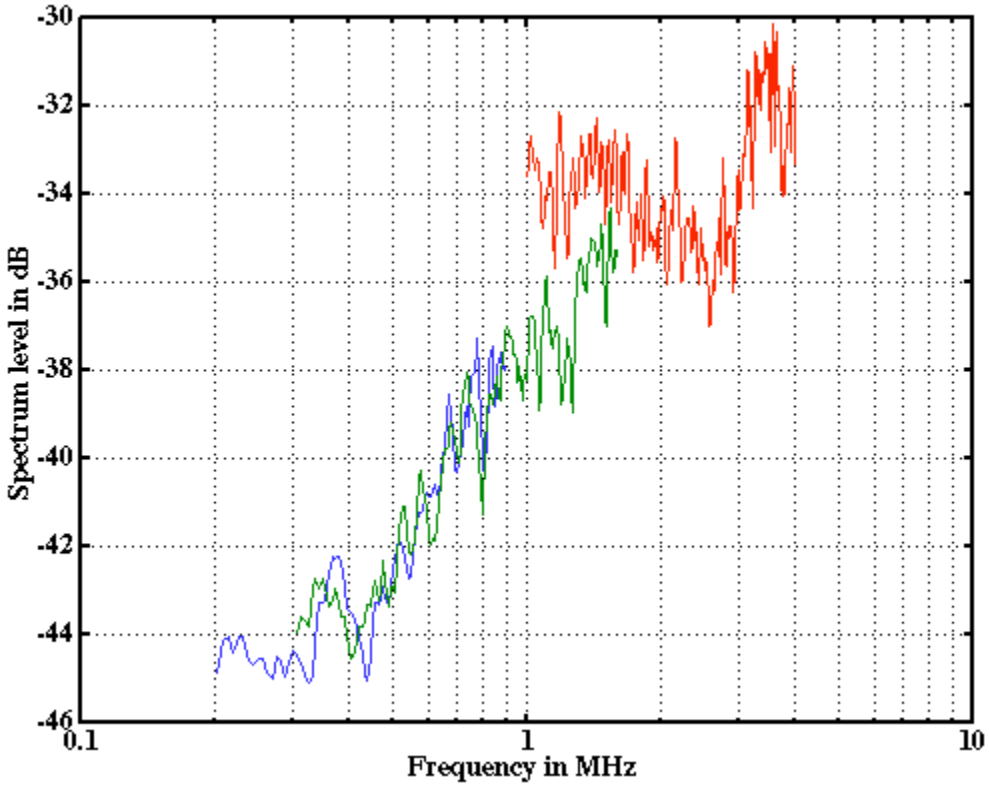

Figure 5. Surface scattering spectra from the three sources averaged over twelve bottom patches. Each spectrum has been normalized by the system response obtained by surface reciprocity. No corrections for effective ensonified area have been made in this data. The grazing angle is 20°.

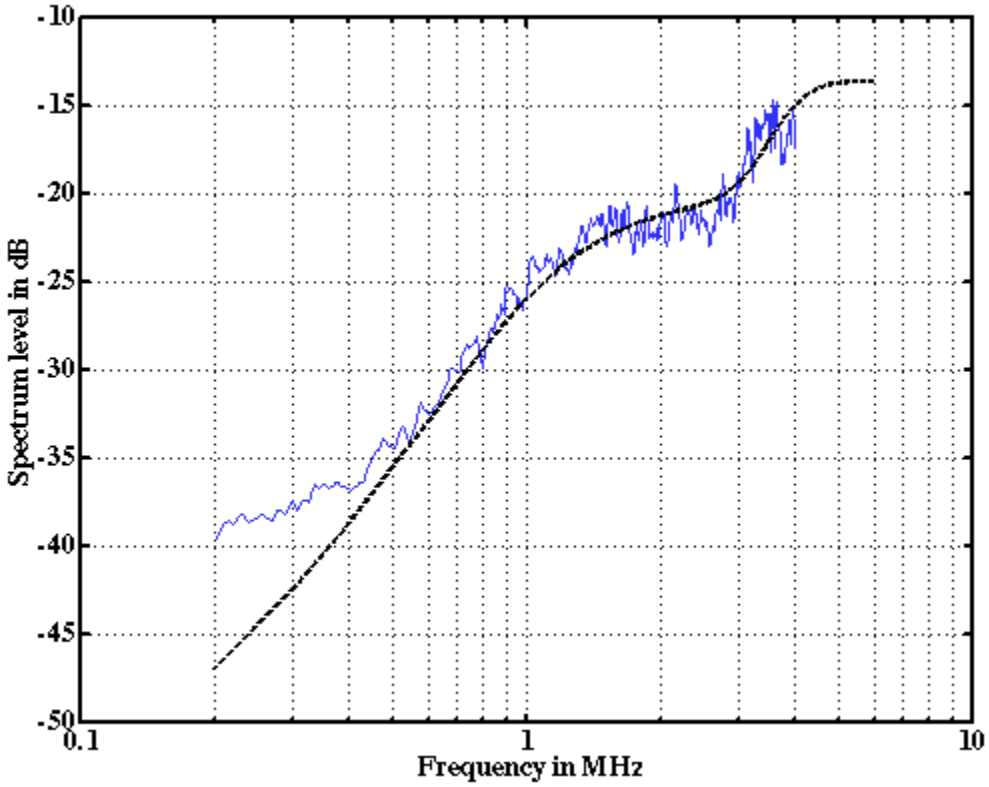

Figure 6. Composite backscattering spectrum from a sandy bottom at 20° grazing angle. The raw spectra have been corrected for relative areal changes over frequency from the finite apertures of the transducers. Where the spectra from the three sources overlapped in frequency, the estimates were averaged to form a single composite spectral estimate. Also shown (dashed curve) is the sand grain model of Sheng (1991) for a grain size of 0.25 mm diameter. The model has been adjusted vertically to obtain a qualitative agreement with the scattering spectrum.

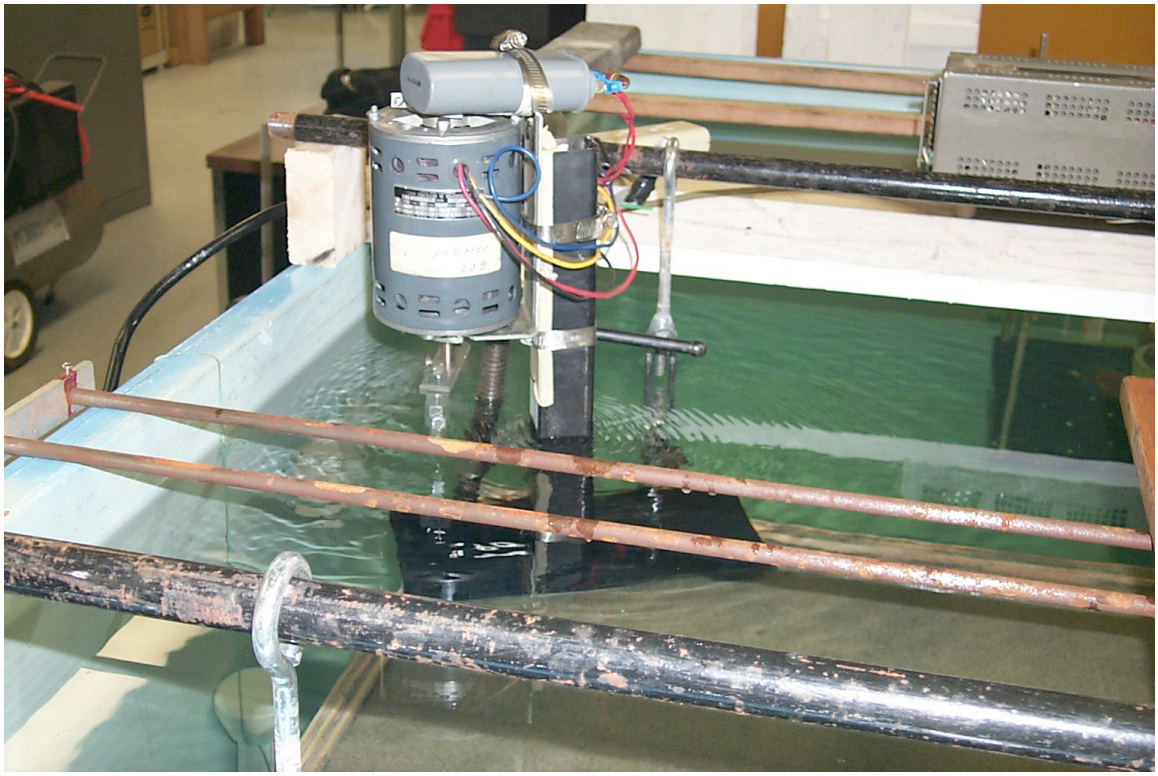

Figure 7. Photograph of compaction apparatus formed from a eccentrically-weighted motor clamped to the box holding the sand. The sand was noticeably firmer to the touch after only one hour of compaction; the motor was run for 12 hours total over two days.

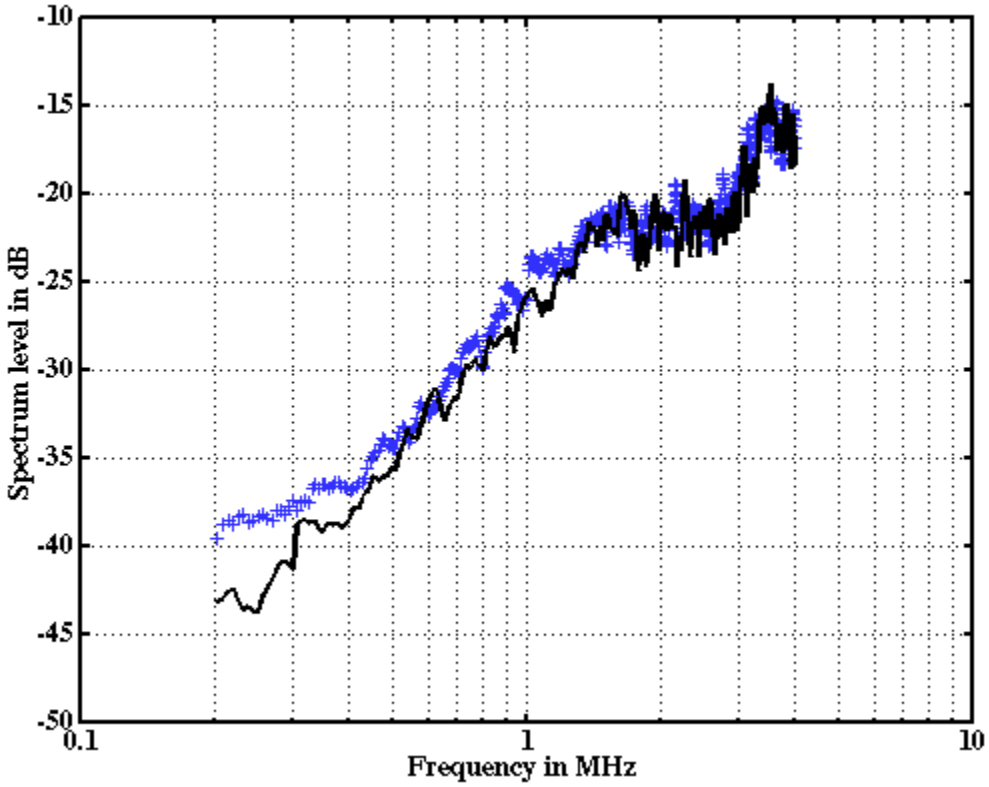

Figure 8. Comparison of the corrected composite surface scattering echo spectra for compacted (solid line) and un-compacted (crosses) sand beds. Minor offsets in level are probably the result of the small changes in the slant range due to packing the sand bed. Grazing angle is 20°.

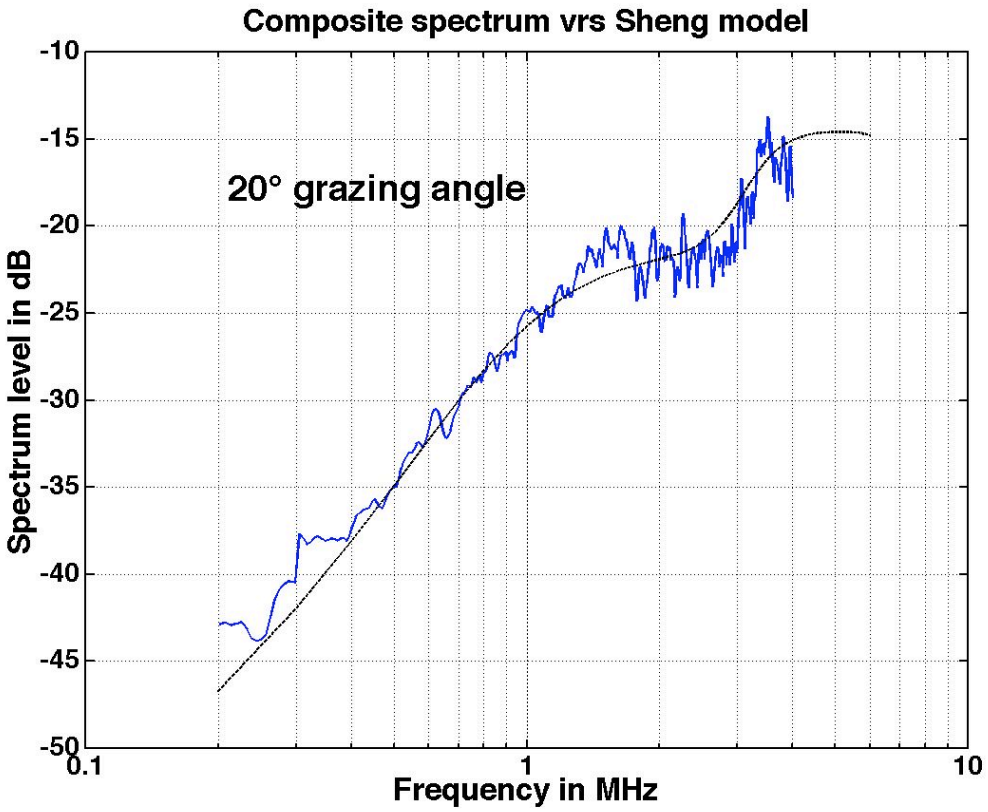

Figure 9. Comparison of the compacted sand backscattering spectrum to the Sheng model at 20° grazing angle. Reasonably good agreement is found above about 500 kHz.

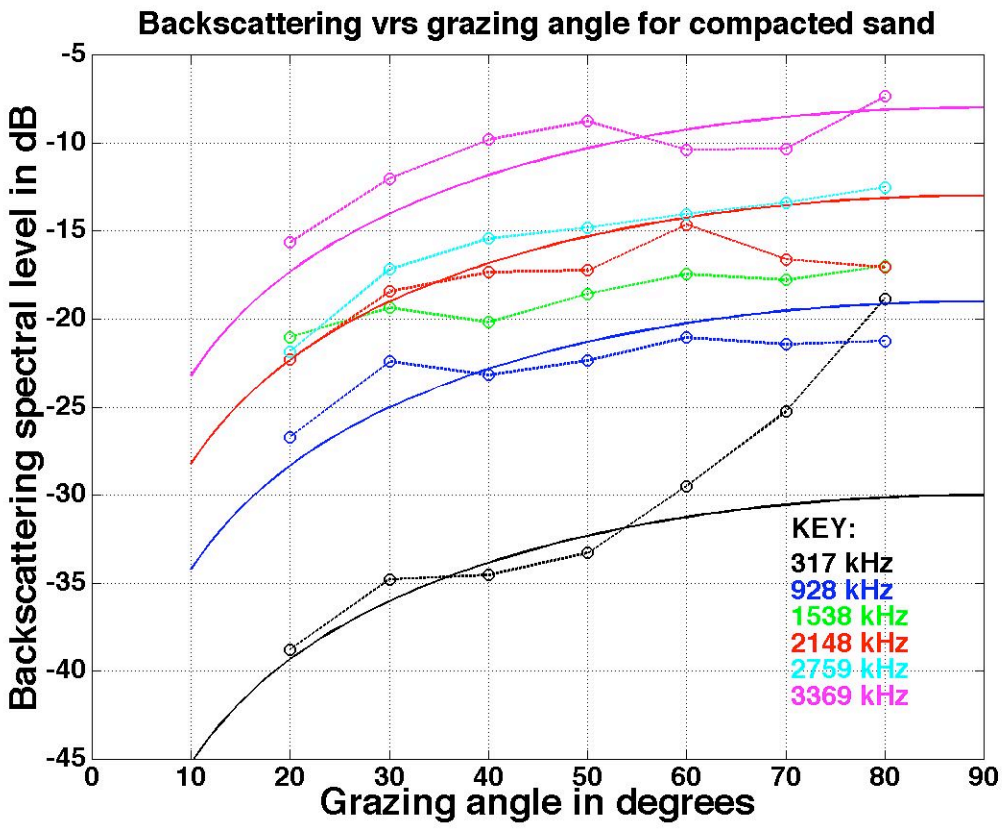

Figure 10. Plots of measured backscattering at selected frequencies versus grazing angle. Each point represents one (smoothed) spectral point. The smooth curves are Lambert's Rule arbitrarily scaled in level and overlaid to illustrate the behavior expected if this Rule applied to these data. Note the departure from Lambert's Rule above about 50° grazing angle at the lowest frequency shown. Compare this behavior with Fig. 5 from Ivakin and Lysanov (1981).

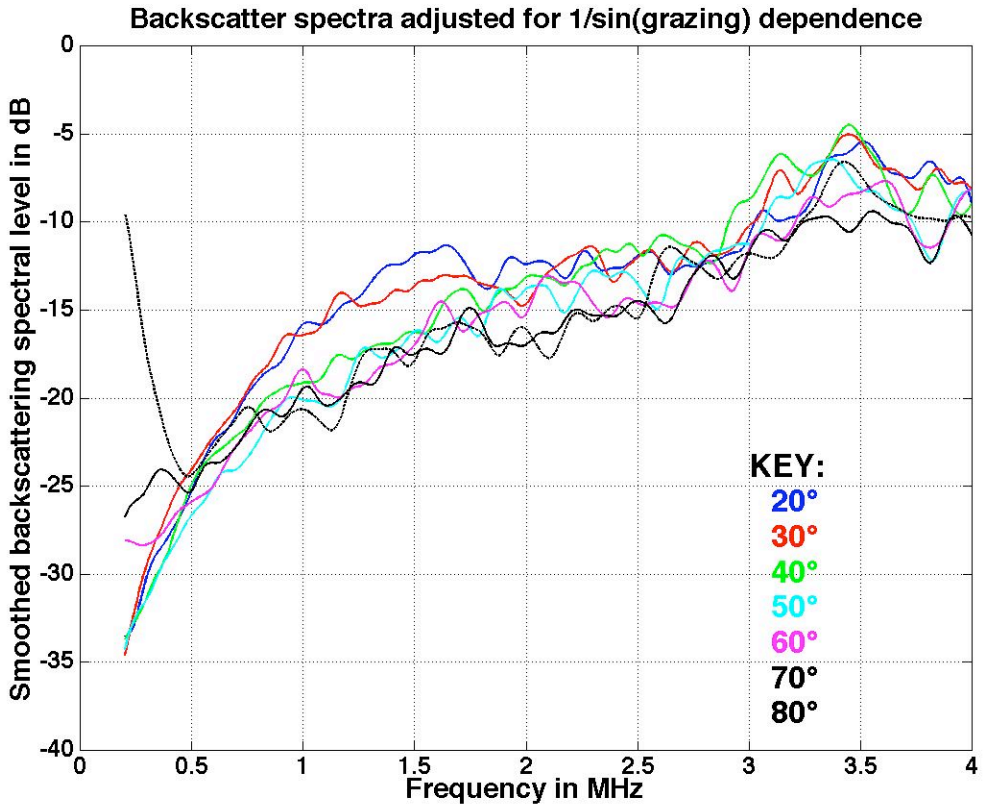

Figure 11. Plots of the measured backscattering spectra at grazing angles from 20° to 80°, corrected by Lambert's Rule. If scattering is consistent with the pseudo-model, then the spectra should overlap. Significant departures are seen both at low frequencies (below ca. 500 kHz) and at certain grazing angles (at or below critical incidence).